

**Science**

 AAAS

## Negative Refraction at Visible Frequencies

Henri J. Lezec, *et al.*

*Science* **316**, 430 (2007);

DOI: 10.1126/science.1139266

**The following resources related to this article are available online at [www.sciencemag.org](http://www.sciencemag.org) (this information is current as of November 7, 2007):**

**Updated information and services**, including high-resolution figures, can be found in the online version of this article at:

<http://www.sciencemag.org/cgi/content/full/316/5823/430>

**Supporting Online Material** can be found at:

<http://www.sciencemag.org/cgi/content/full/1139266/DC1>

This article **cites 25 articles**, 3 of which can be accessed for free:

<http://www.sciencemag.org/cgi/content/full/316/5823/430#otherarticles>

This article has been **cited by** 4 article(s) on the ISI Web of Science.

This article has been **cited by** 1 articles hosted by HighWire Press; see:

<http://www.sciencemag.org/cgi/content/full/316/5823/430#otherarticles>

This article appears in the following **subject collections**:

Physics, Applied

[http://www.sciencemag.org/cgi/collection/app\\_physics](http://www.sciencemag.org/cgi/collection/app_physics)

Information about obtaining **reprints** of this article or about obtaining **permission to reproduce this article** in whole or in part can be found at:

<http://www.sciencemag.org/about/permissions.dtl>

# Negative Refraction at Visible Frequencies

Henri J. Lezec,<sup>1,2\*</sup>† Jennifer A. Dionne,<sup>1\*</sup> Harry A. Atwater<sup>1</sup>

Nanofabricated photonic materials offer opportunities for crafting the propagation and dispersion of light in matter. We demonstrate an experimental realization of a two-dimensional negative-index material in the blue-green region of the visible spectrum, substantiated by direct geometric visualization of negative refraction. Negative indices were achieved with the use of an ultrathin Au-Si<sub>3</sub>N<sub>4</sub>-Ag waveguide sustaining a surface plasmon polariton mode with antiparallel group and phase velocities. All-angle negative refraction was observed at the interface between this bimetal waveguide and a conventional Ag-Si<sub>3</sub>N<sub>4</sub>-Ag slot waveguide. The results may enable the development of practical negative-index optical designs in the visible regime.

When a beam of light enters a material from vacuum or air at non-normal incidence, it undergoes refraction—a change in its direction of propagation. The angle of refraction depends on the absolute value of the refractive index of the medium, according to Snell's law. For all naturally occurring substances, the beam is deflected to the opposite side of the interface normal, and the refractive index is taken to be positive.

In 1968, Veselago studied a theoretical material with simultaneously negative electric permittivity  $\epsilon$  and magnetic permeability  $\mu$ , and predicted that it would have a negative index of refraction  $n$  (1). Light crossing the boundary between such a medium and one with a positive refractive index would refract to the same side of the normal. Such a deflection, termed negative refraction, was predicted to lead to a variety of enabling applications, most notably subwavelength focusing with resolution well below the diffraction limit (2).

Considerable research has been devoted to developing artificial electromagnetic media with negative  $n$  resulting from negative  $\epsilon$  and  $\mu$  (3, 4). Such media, known as negative-index materials (NIMs), were first implemented at microwave frequencies on the order of 10 GHz by means of periodic assemblies of millimeter-scale split-ring resonators and wires (5, 6). Negative values of  $\mu$  and  $\epsilon$  were simultaneously achieved via, respectively, the resonant capacitive-inductive response of the split-rings (7) and the effective plasma response of the wire lattice determined by mutual inductance (8). All-angle negative refraction in two dimensions was then demonstrated by direct observation of plane-wave refraction through prism-shaped segments of such assemblies (5, 6).

Efforts are now directed toward scaling down NIMs for operation at optical frequencies (9, 10). So far, structures have been limited to one (11–14) or a few (15) layers of discrete resonator elements. Transmission and reflection spectra measured with out-of-plane illumination

enable retrieval of  $\epsilon$ ,  $\mu$ , and  $n$  (16); in this manner, negative indices were inferred at infrared frequencies (11–13, 15) and recently at the red end of the visible spectrum (14). However, because the thickness of such NIMs is substantially smaller than the free-space wavelength, the interaction volume with the incident radiation presumably remains too small to induce angular deviations of light with sufficient amplitude to provide direct evidence of negative refraction.

Here, we demonstrate a planar NIM at visible frequencies. It is based on the proposal that a suitably designed metal-insulator-metal (MIM) waveguide can act as a two-dimensional NIM characterized by an effective  $\epsilon$  and  $\mu$  that are both negative when averaged over the thickness of the waveguide (17–21). The negative response arises from the in-plane isotropic dispersion properties of a transverse magnetic (TM) mode involving coupled surface plasmon polaritons (SPPs) at each metal-dielectric interface. For frequencies above the surface plasmon resonance frequency  $\omega_{\text{SP}}$ , but below the bulk plasmon frequency  $\omega_{\text{p}}$ , the dispersion curve exhibits negative slope leading to antiparallel group and phase velocities, meaning that the energy and phase fronts propagate in opposite directions. Such a mode then behaves as if it had a negative index of refraction (22). If it is the only sustained mode, this index can be considered to be equivalent to

the effective index of refraction of the two-dimensional medium itself.

In this experiment, we used two MIM waveguides cascaded in series to directly visualize negative refraction. The first waveguide is designed to sustain propagation of only a single negative-index mode over a broad subset of the visible frequency range. The second waveguide is tailored to sustain propagation of only positive-index modes over the same range. Structures are fabricated by applying a sequence of thermal evaporation and focused ion beam milling steps to both sides of a suspended Si<sub>3</sub>N<sub>4</sub> membrane.

Figure 1A illustrates the dispersion properties of a planar Ag-Si<sub>3</sub>N<sub>4</sub>-Ag waveguide with dielectric core thickness  $t = 500$  nm. Modal properties were calculated via numerical solution of Maxwell's equations assuming perfect coupling between each metal-dielectric interface (23, 24). The waveguide sustains a number of TM modes (25), each identified with the closest related mode of a parallel-plate waveguide with perfect metal surfaces (26). Most modes lie to the left of the light line  $\omega = ck_0/n_d$ , where  $n_d$  is the refractive index of the core and  $k_0 = 2\pi/\lambda_0$ . These “photonic” modes are characterized by a propagation constant  $\beta < n_d k_0$ . In addition, an SPP mode characterized by  $\beta > n_d k_0$  and corresponding to degenerate, cutoff-free TM<sub>0</sub> and TM<sub>1</sub> modes is present to the right of the light line. Over the entire visible range ( $400 \text{ nm} < \lambda_0 < 700 \text{ nm}$ ), all allowed modes obey the condition  $d\omega/d\beta \geq 0$ , corresponding to a positive refractive index of light in the waveguide.

As the dielectric core thickness  $t$  is reduced, the cutoff energy of each photonic mode increases. For  $t = 50$  nm, a single allowed mode remains in the visible range: the TM<sub>0</sub> SPP mode [the TM<sub>1</sub> SPP mode of Fig. 1A is completely attenuated by absorption (24)]. The dispersion curve of this mode (Fig. 1B, gray curve) exhibits a negative slope ( $d\omega/d\beta < 0$ ) and hence negative-index behavior over the ultraviolet frequency range  $\omega_{\text{SP}}^{\text{Ag-Si}_3\text{N}_4} < \omega < \omega_{\text{p}}^{\text{Ag}}$  (where  $\omega_{\text{SP}}^{\text{Ag-Si}_3\text{N}_4}$  and  $\omega_{\text{p}}^{\text{Ag}}$  are the resonant frequencies of the Ag-Si<sub>3</sub>N<sub>4</sub> surface plasmon and the Ag bulk plas-

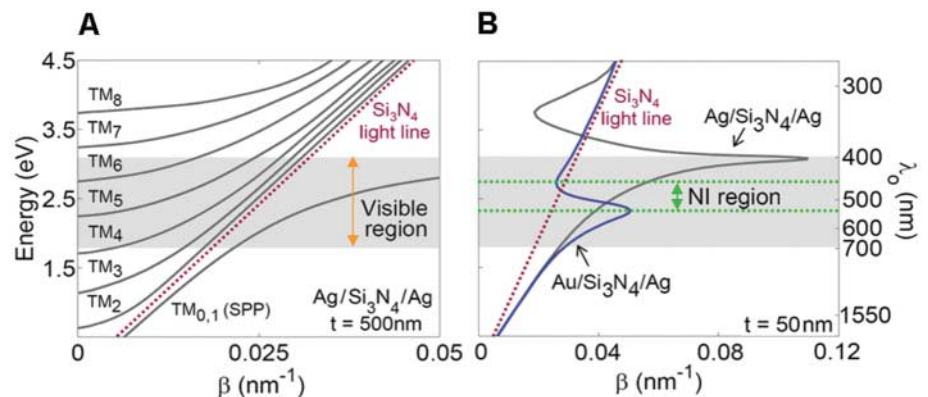


**Fig. 1.** Implementation of positive- and negative-index MIM waveguides. (A) Calculated dispersion curves for an Ag-Si<sub>3</sub>N<sub>4</sub>-Ag waveguide with a dielectric core thickness  $t = 500$  nm. (B) Calculated dispersion curves for Ag-Si<sub>3</sub>N<sub>4</sub>-Ag and Au-Si<sub>3</sub>N<sub>4</sub>-Ag waveguides with  $t = 50$  nm.

<sup>1</sup>Thomas J. Watson Laboratory of Applied Physics, California Institute of Technology, Pasadena, CA 91125, USA.

<sup>2</sup>Centre National de la Recherche Scientifique, 3 rue Michel-Ange, 75794 Paris Cedex 16, France.

\*These authors contributed equally to this work.

†To whom correspondence should be addressed. E-mail: lezec@caltech.edu

mon, respectively). By swapping Ag with Au in one of the cladding layers, this region of negative slope can be shifted to the interval  $470 \text{ nm} < \lambda_0 < 530 \text{ nm}$ , well within the visible (Fig. 1B, blue curve). Calculated losses for the resulting negative-index mode in this Au-Si<sub>3</sub>N<sub>4</sub>-Ag waveguide indicate a characteristic power attenuation distance of  $\sim 50 \text{ nm}$ , as well as an average figure of merit  $\text{FOM} = |\text{Re}(n)/\text{Im}(n)| \sim 4$ . This FOM appears somewhat higher than those summarized (9, 10) for recent resonator-based negative-index metamaterials operating at the onset between the visible and infrared regimes (where quoted FOMs range from 3 at  $\lambda_0 = 1.4 \mu\text{m}$  to 0.5 at  $\lambda_0 = 780 \text{ nm}$ ).

Figure 2A displays a cross section of the experimental device used to demonstrate negative refraction. An Au-Si<sub>3</sub>N<sub>4</sub>-Ag waveguide (W1) with a thin dielectric core ( $t_1 = 50 \text{ nm}$ ) is positioned between two identical Ag-Si<sub>3</sub>N<sub>4</sub>-Ag waveguides (W2) with thick dielectric cores ( $t_2 = 500 \text{ nm}$ ). The 100-nm thicknesses of the Ag and Au cladding layers are substantially larger than the mode skin depth (27). In addition, a 200-nm-thick layer of Al is deposited on each side of the waveguide to ensure complete opacity of the respective top and bottom cladding layers. Slits of subwavelength width ( $w = 400 \text{ nm}$ ) couple light into and out of the waveguide (28). The input slit is illuminated at normal incidence with TM-polarized laser light ( $H$ -field parallel to the slit). The output slit is imaged using a  $50\times$  objective coupled to a liquid nitrogen-cooled charge-coupled device camera.

Direct characterization of positive or negative refraction is achieved by shaping W1 into a prism in the plane of propagation (Fig. 2B). A guided mode is first launched in W2 via the input slit at normal incidence on the leading edge of the prism, where it excites a SPP mode that propagates through W1 with effective index  $n_1$ . The SPP mode in turn impinges on the slanted interface between W1 and W2, at angle  $\varphi_1$ . The mode is then refracted at an angle  $\varphi_2$  into a guided mode of W2 with effective index  $n_2$ . We estimate  $\varphi_2$  from the projected position of the mode on the output slit and use Snell's law (22) to determine the ratio  $n_1/n_2 = \sin(\varphi_2)/\sin(\varphi_1)$ .

Refraction results obtained at wavelengths  $\lambda_0 = 685 \text{ nm}$  and  $514 \text{ nm}$  are illustrated in Fig. 3. These two wavelengths fall, respectively, in the calculated positive- and negative-index regions of W1 (Fig. 1B).

Figure 3A evaluates waveguide transmission through W2 in the absence of a prism. At both wavelengths, a clear image of the input slit is projected onto the output slit, consistent with previous observations of low lateral mode divergence within MIM waveguides (28).

Figure 3B illustrates the effect of introducing two symmetric prisms of W1 into W2. The diagonal edges of both prisms are parallel and form an angle of  $7^\circ$  with respect to the wavefront launched by the input slit. Vertical displacement of the incident beam is proportional to the angle

**Fig. 2.** Schematic diagram of structure fabricated to demonstrate in-plane negative refraction. A prism-shaped segment of Au-Si<sub>3</sub>N<sub>4</sub>-Ag waveguide with variable dielectric core thickness  $t_1$  and edge angle  $\theta$  ("W1") is embedded in an Ag-Si<sub>3</sub>N<sub>4</sub>-Ag waveguide of fixed core thickness  $t_2 = 500 \text{ nm}$  ("W2"). Two slits extending into the waveguide core (nominal width  $w = 400 \text{ nm}$ ) are used to excite and intercept, respectively, a guided electromagnetic mode. **(A)** Cross section showing path of light through structure (white arrows). **(B)** Corresponding plan view showing guided mode at two different frequencies illustrating, respectively, positive refraction (red arrow) and negative refraction (green arrow).

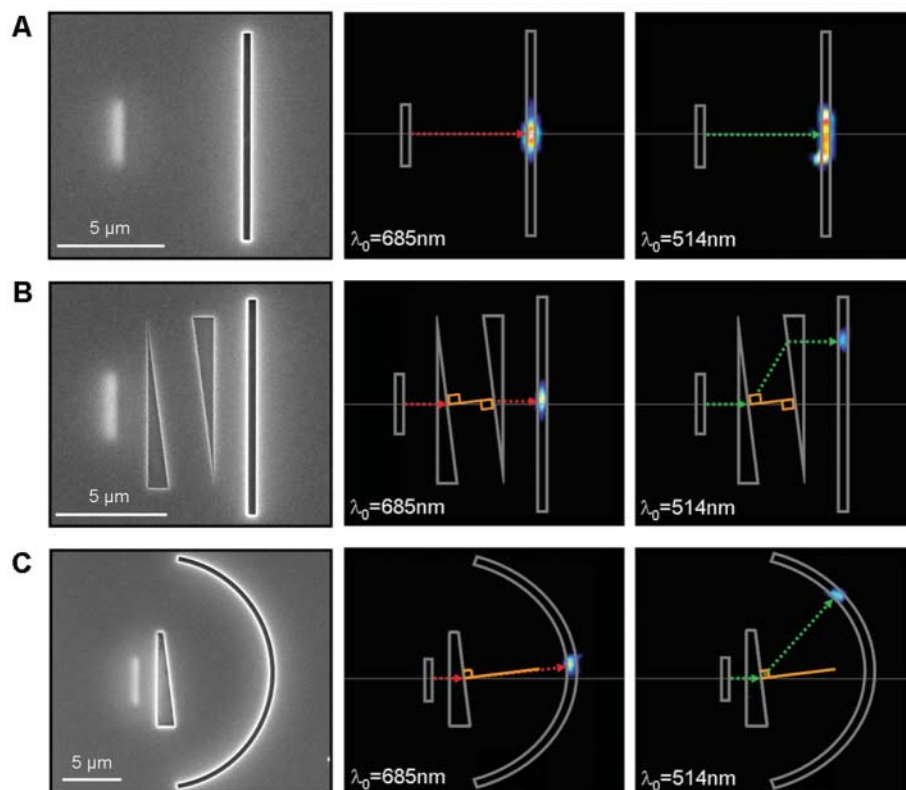
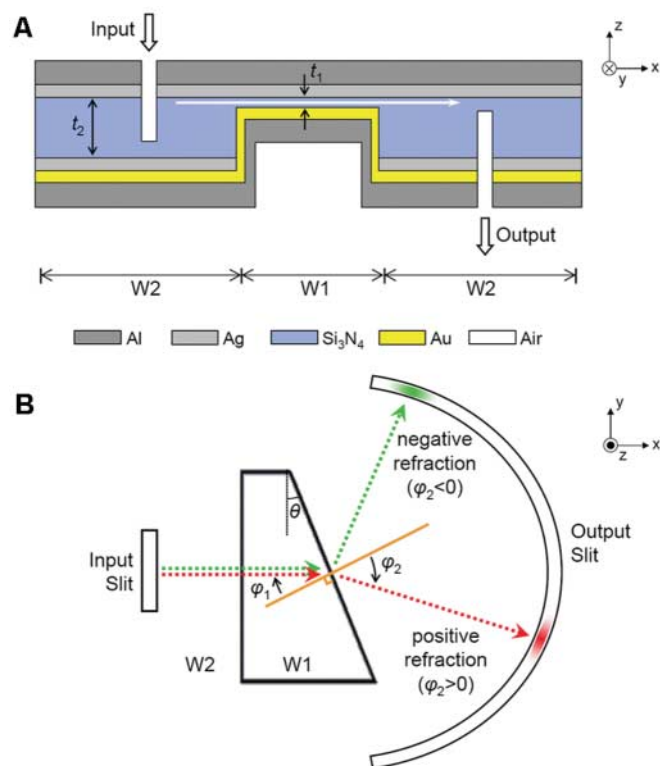


**Fig. 3.** Direct visualization of in-plane negative refraction. Three waveguide configurations are explored: **(A)** W2 alone, **(B)** two prisms of W1 ( $t_1 = 50 \text{ nm}$ ,  $\theta = 7^\circ$ ) embedded in W2, and **(C)** one prism of W1 ( $t_1 = 50 \text{ nm}$ ,  $\theta = 7^\circ$ ) embedded in W2. Left column: Scanning electron micrograph image of output side. Input slit position is revealed by electron transparency. Center and right columns: Optical microscope image of output side, given input-side illumination at  $\lambda_0 = 685 \text{ nm}$  and  $514 \text{ nm}$ , respectively.

of refraction at the first angled interface,  $\varphi_2$ . The double-prism configuration corrects for differences in the optical path length, ensuring that the mode experiences uniform absorption during its transit from input slit to output slit. At  $\lambda_0 = 685$  nm, the observed output-spot position indicates positive refraction at both slanted interfaces between W1 and W2, with an angle  $\varphi_2 = +0.1^\circ$ . In contrast, at  $\lambda_0 = 514$  nm, the output-spot position indicates negative refraction between W1 and W2, with an angle  $\varphi_2 = -51^\circ$ . Given the prism angle  $\varphi_1 = \theta = 7^\circ$ , Snell's law yields an index ratio  $n_1/n_2 = +0.01$  and  $-6.26$  at  $\lambda_0 = 685$  nm and 514 nm, respectively.

Similar trends are observed when a single prism of W1 is placed in the path of the guided mode in W2 (Fig. 3C). The straight output slit of Fig. 3B is replaced with a semicircular slit to ensure that the refracted mode intersects the slit at normal incidence for any refraction angle. At  $\lambda_0 = 685$  nm, the position of the output spot indicates positive refraction at the interface between W1 and W2, with an angle  $\varphi_2 = +0.1^\circ$ . When  $\lambda_0$  is reduced to 514 nm, the output-spot position shifts, indicating negative refraction at the interface between W1 and W2, with an angle  $\varphi_2 = -43.7^\circ$ . Given the incident angle  $\varphi_1 = 7^\circ$ , Snell's law yields an index ratio  $n_1/n_2 = +0.01$  and  $-5.57$  at  $\lambda_0 = 685$  nm and 514 nm, respectively. These values are in good agreement with those measured using the double-prism configuration of Fig. 3B.

To derive the mode index of the thin Au-Si<sub>3</sub>N<sub>4</sub>-Ag waveguide,  $n_1$ , it is necessary to determine the mode index of the surrounding thicker Ag-Si<sub>3</sub>N<sub>4</sub>-Ag waveguide,  $n_2$ . To circumvent the

difficulty of estimating  $n_2$  theoretically, given the prediction of multimodal dispersion properties for W2 (Fig. 1A), we measured  $n_2$  directly by an interferometric technique (22). At  $\lambda_0 = 514$  nm, we obtained  $n_2 = 0.82$ , which implies effective refractive indices for the Au-Si<sub>3</sub>N<sub>4</sub>-Ag waveguides of Fig. 3 that are both large and negative:  $n_1 = -4.6$  and  $-5.1$  for Fig. 3, B and C, respectively. At  $\lambda_0 = 685$  nm, we measured  $n_2 = 0.75$ , yielding a very small positive index  $n_1 = 0.01$  in both cases. The effective index  $n_1$  of a number of prisms with different angles  $\theta$  and dielectric core thicknesses  $t_1$  is summarized in Fig. 4A; data are tabulated for closely spaced free-space wavelengths spanning the predicted negative-index region. In particular, the relative invariance of  $n_1$  as a function of  $\theta$  confirms that our structures indeed obey all-angle in-plane refraction according to Snell's law (22). Finally, we plotted the full set of refraction data  $n_1(\lambda)$  as  $\lambda(\beta)$ , yielding the dispersion behavior of the guided mode in the prism (Fig. 4B); the dispersion curve clearly presents a negative slope for  $\lambda_0$  between 476 and 514 nm, in good agreement with calculations.

Using specially tailored metal-insulator-metal waveguides, we have realized a planar material with an effective negative refractive index in the blue-green region of the visible spectrum. Isotropic negative refraction in two dimensions is directly observed; in resonator-based metamaterials, such a measurement has so far been achieved only in the microwave regime. Nonresonant negative-index behavior is achieved over a broad  $\sim 50$ -nm ( $\sim \lambda_0/10$ ) wavelength range, which can in principle be further extended by increasing the dielectric

constant of the waveguide core. The structure is straightforward to fabricate because its performance depends only on the plasmonic properties of two smooth metal-dielectric interfaces and a single critical dimension adjusted to ensure monomode behavior: the thickness of a silicon nitride film. The approach appears promising for straightforward two-dimensional implementation of theoretically predicted negative refraction-based devices, such as a perfect lens capable of non-quasistatic, far-field focusing with subwavelength resolution (2). In addition, the inherent simplicity of the structure hints at its potential as a building block for future artificial media capable of all-angle negative refraction in three dimensions (18, 19).

## References and Notes

- V. G. Veselago, *Sov. Phys. Usp.* **10**, 509 (1968).
- J. B. Pendry, *Phys. Rev. Lett.* **85**, 3966 (2000).
- S. A. Ramakrishna, *Rep. Prog. Phys.* **68**, 449 (2005).
- C. M. Soukoulis, M. Kafesaki, E. N. Economou, *Adv. Mater.* **18**, 1941 (2006).
- R. A. Shelby, D. R. Smith, S. Schultz, *Science* **292**, 77 (2001).
- A. A. Houck, J. B. Brock, I. L. Chuang, *Phys. Rev. Lett.* **90**, 137401 (2003).
- J. B. Pendry, A. J. Holden, D. J. Robbins, W. J. Stewart, *IEEE Trans. Microw. Theory Tech.* **47**, 2075 (1999).
- J. B. Pendry, A. J. Holden, W. J. Stewart, I. Youngs, *Phys. Rev. Lett.* **76**, 4773 (1996).
- V. Shalaev, *Nat. Photonics* **1**, 41 (2007).
- C. M. Soukoulis, S. Linden, M. Wegener, *Science* **315**, 47 (2007).
- S. Zhang *et al.*, *Phys. Rev. Lett.* **95**, 137404 (2005).
- V. M. Shalaev, *Opt. Lett.* **30**, 3356 (2005).
- G. Dolling, C. Enkrich, M. Wegener, C. M. Soukoulis, S. Linden, *Science* **312**, 892 (2006).
- G. Dolling, M. Wegener, C. M. Soukoulis, S. Linden, *Opt. Lett.* **32**, 53 (2007).
- G. Dolling, M. Wegener, S. Linden, *Opt. Lett.* **32**, 551 (2007).
- D. R. Smith, S. Schultz, P. Markos, C. M. Soukoulis, *Phys. Rev. B* **65**, 195104 (2002).
- P. Tournois, V. Laude, *Opt. Commun.* **137**, 41 (1997).
- G. Shvets, *Physica B* **338**, 338 (2003).
- G. Shvets, *Phys. Rev. B* **67**, 035109 (2003).
- A. Alu, N. Engheta, *J. Opt. Soc. Am. B* **23**, 571 (2006).
- H. Shin, S. H. Fan, *Phys. Rev. Lett.* **96**, 073907 (2006).
- See supporting material on Science Online.
- J. A. Dionne, L. A. Sweatlock, H. A. Atwater, A. Polman, *Phys. Rev. B* **72**, 075405 (2005).
- J. A. Dionne, L. A. Sweatlock, H. A. Atwater, A. Polman, *Phys. Rev. B* **73**, 035407 (2006).
- Transverse electric (TE) modes also exist but are not excited given the incident polarization.
- K. Y. Kim, Y. K. Cho, H. S. Tae, J. H. Lee, *Opt. Express* **14**, 320330 (2006).
- For 470 nm  $< \lambda_0 < 530$  nm, calculated skin depths in the Ag and Au layers do not exceed 21.5 nm and 30.0 nm, respectively.
- J. A. Dionne, H. J. Lezec, H. A. Atwater, *Nano Lett.* **6**, 1928 (2006).
- Supported by a National Defense Science and Engineering Graduate Fellowship administered by the Army Research Office (J.A.D.) and by the Air Force Office of Scientific Research under Plasmon Multidisciplinary University Research Initiative FA9550-04-1-0434. We thank L. Sweatlock, D. Pacifici, R. Walters, B. Kayes, N. Vu, G. Derose, and A. Scherer for engaging discussions and technical assistance.

## Supporting Online Material

www.sciencemag.org/cgi/content/full/1139266/DC1

SOM Text

Figs. S1 and S2

References

26 December 2006; accepted 12 March 2007

Published online 22 March 2007;

10.1126/science.1139266

Include this information when citing this paper.

**Fig. 4.** Measured mode index (A) and mode dispersion (B) of Au-Si<sub>3</sub>N<sub>4</sub>-Ag prisms with various values of  $t_1$  and  $\theta$ , for frequencies spanning the negative-index region. The calculated dispersion curves for limiting cases  $t = 150$  nm and  $t = 50$  nm are also included.

